

ORIGINAL ARTICLE

Angiography

## Coronary Magnetic Resonance Angiography for Assessment of the Stent Lumen: A Phantom Study

---

David Maintz,<sup>1,3,\*</sup> Rene M. Botnar,<sup>1,2</sup>  
Roman Fischbach,<sup>3</sup> Walter Heindel,<sup>3</sup>  
Warren J. Manning,<sup>1</sup> and Matthias Stuber<sup>1,2</sup>

<sup>1</sup>Cardiac MR Center, Beth Israel Deaconess Medical Center and Harvard Medical School, Boston, Massachusetts

<sup>2</sup>Philips Medical Systems, Best, The Netherlands

<sup>3</sup>Department of Clinical Radiology, University of Münster, Münster, Germany

### ABSTRACT

*Purpose:* To evaluate the feasibility of visualizing the stent lumen using coronary magnetic resonance angiography in vitro.

*Material and methods:* Nineteen different coronary stents were implanted in plastic tubes with an inner diameter of 3 mm. The tubes were positioned in a plastic container filled with gel and included in a closed flow circuit (constant flow 18 cm/sec). The magnetic resonance images were obtained with a dual inversion fast spin-echo sequence. For intraluminal stent imaging, subtraction images were calculated from scans with and without flow. Subsequently, intraluminal signal properties were objectively assessed and compared.

*Results:* As a function of the stent type, various degrees of in-stent signal attenuation were observed. Tantalum stents demonstrated minimal intraluminal signal attenuation. For nitinol stents, the stent lumen could be identified, but the intraluminal signal was markedly reduced. Steel stents resulted in the most pronounced intraluminal signal voids.

*Conclusions:* With the present technique, radiofrequency penetration into the stents is strongly influenced by the stent material. These findings may have important implications for future stent design and stent imaging strategies.

\*Corresponding author. Department of Clinical Radiology, University of Muenster, Albert-Schweitzer-Str. 33, 48129 Münster, Germany. Fax: +49-251-83-47317; E-mail: maintz@uni-muenster.de

**Key Words:** *Stents and prostheses; Magnetic resonance angiography; Coronary magnetic resonance angiography; Artifacts*

## INTRODUCTION

Coronary stenting is currently the most widely used percutaneous coronary intervention with an estimated 500,000 stents implanted in the United States in 1998.<sup>[1]</sup> The main benefit of stenting when compared with balloon-angioplasty alone is a reduction of the restenosis-rate. Nevertheless, in-stent restenosis remains a relatively common clinical scenario.<sup>[2–5]</sup> If clinical symptoms suggest in-stent restenosis, x-ray coronary angiography is currently considered the gold standard for the evaluation of stent integrity. Since conventional x-ray angiography has several disadvantages, including a small risk of serious complications, the need for an iodinated contrast agent, and radiation exposure, a noninvasive imaging method for direct assessment of stent lumen integrity would be desirable.<sup>[6]</sup>

Currently, the majority of coronary artery stents are nonferromagnetic and are considered to be magnetic resonance (MR) safe,<sup>[7]</sup> but stents remain the source of local image artifacts, which impede the diagnostic information on MR images. While various coronary artery stents have been evaluated in vitro with regard to the total volume of their artifacts as a function of different imaging sequences,<sup>[8]</sup> to our knowledge, the visualization of the stent lumen has not previously been reported. Therefore, we implemented an MR imaging methodology to quantify in-stent signal attenuation among 19 commercial coronary stents.

## MATERIAL AND METHODS

### Evaluated Stents and Experimental Setup

Nineteen different (material and/or design) coronary artery stents were studied. The name, manufacturer, material, length, and nominal diameter of the stents are summarized in Table 1. Seventeen stents were made of stainless surgical steel (316L), and one each of nitinol (Radius) and of tantalum (Wiktor). Some steel stents were coated with various materials including gold, phosphorylcholin, carbon, or carbon like diamond (Table 1).

The stents were implanted in plastic tubes with a length of 23 cm and an inner diameter of 3 mm to simulate placement in a 3 mm coronary artery with no residual stenosis. The tubes were positioned in a plastic container (size 28 × 18 × 10 cm<sup>3</sup>) filled with gel and connected to a

closed flow circuit. The flow was adjusted to a constant 18 cm/sec (approximating peak coronary flow velocity).

The volume of the stent material and the ratio of that volume to the total volume of the stented part of the vessel were quantified from the mass and the specific weight of the stents (volume = mass/density). Hereby, the values for the densities of stainless steel, tantalum, and nitinol were 7850, 16,650, and 6500 kg/m<sup>3</sup>. The density of the thin layers of coating materials (gold, phosphorylcholin, carbon, etc.) were neglected for the present analysis.

### MR Imaging

Images were acquired on a 1.5 T whole-body MR system (Gyrosan ACS-NT, Philips Medical Systems, Best, The Netherlands) equipped with cardiac software (CPR6) and a PowerTrack 6000 gradient system (strength 23 mT/m; rise time 220 msec). A cardiac synergy coil (two anterior and three posterior elements) was used for signal reception. Localization of the stented “vessel” was performed with a multislice, two-dimensional, segmented gradient echo scout sequence (TR = 11 msec, TE = 2.4 msec, 256 × 128 matrix, 450 mm field of view (FOV), 10 mm slice thickness, 5 mm slice gap, ~1 min acquisition time) with nine transverse, nine coronal, and nine sagittal acquisitions. Coronary magnetic resonance angiography (MRA) was performed with a previously described black-blood coronary MRA technique.<sup>[9]</sup> The imaging sequence was an ECG-triggered (artificial ECG set at 70 beats/min), three-dimensional fast spin-echo sequence with a linear *k*-space acquisition scheme, 28 msec TE, and a TR of two RR intervals. A 512 scan matrix was sampled with an echo train length of 17 and an interecho spacing of 7.6 msec, resulting in an acquisition window of 130 msec per RR interval. Other parameters included half-Fourier sampling, FOV 360 mm with a resultant in-plane voxel size of 700 μm and two signal averages. A dual inversion prepulse was applied immediately after the detection of the R-wave of the ECG. A 16 mm thick three-dimensional slab was imaged consisting of eight adjacent slices of 2 mm slice thickness each. Sixteen slices with a slice thickness of 1 mm were reconstructed using zero-filling in *k<sub>z</sub>* direction. The same stents were imaged twice, with flow and without flow. Subsequently, both image data sets were subtracted from one another.

**Table 1**  
*Commercial Name, Manufacturer, Material, Length, Strut Dimensions, Weight, and Volume of the Examined Stents*

Name	Manufacturer	Material	Length (mm)	Strut-Dimensions (mm)	Weight (g)	Volume (cm <sup>3</sup> )
Wiktor Radius	Medtronic, Düsseldorf, Germany Boston Scientific, Ratingen, Germany	Tantal Nitinol	29 14	0.127 0.102–0.109	0.0476 0.0217	0.0000985 0.0002384
ACS RX Multi-link	Guidant, Giessen, Germany	Stainless steel 316L	29	0.091–0.124	0.0230	0.00014646
Crossflex	Cordis, Haan, Germany	Stainless steel 316L	23	0.14	0.0379	0.0002099
Sirius Carbo-s-tent	Sorin Biomedica, Saluggia, Italy	Stainless steel 316L + Carbon-coating + 2 Platinum markers	15	0.070	0.0144	0.0001222
ML Tetra	Guidant, Giessen, Germany	Stainless steel 316L	13	0.091–0.124	0.0200	0.0001959
Herculink	Guidant, Giessen, Germany	Stainless steel 316L	18	0.168 × 0.178	0.0548	0.0003878
ML Tristar	Guidant, Giessen, Germany	Stainless steel 316L	18	0.091–0.124	0.0286	0.0002024
V-Flex Plus	Cook, Mönchengladbach, Germany	Stainless steel 316L	12	0.076	0.0104	0.0001104
Be-Stent	Medtronic, Düsseldorf, Germany	316L + Platinum markers	12	0.07–0.095	0.0098	0.000104
BiodivYsio	Biocompatibles, Farnham, UK	Stainless steel 316L + Phosphorylcholine-coating	18	0.091	0.0170	0.0001475
Flex AS	Phytis, Berlin, Germany	Stainless steel 316L + DLC-coating	12	0.08–0.09	0.0096	0.00012229
Jostent Flex	Jomed, Rangendingen, Germany	Stainless steel 316L	20	0.09	0.0198	0.0001261
Palmaz-Crown	Cordis, Haan, Germany	Stainless steel 316L	22	0.069	0.0280	0.0001525
NIR Primo	Boston Scientific, Ratingen, Germany	Stainless steel 316L	33	0.102–0.109	0.0294	0.0001134
Palmaz Bx-Velocity	Cordis, Haan, Germany	Stainless steel 316L	14	0.064	0.0230	0.0002092
Jostent Stent-Graft	Jomed, Rangendingen, Germany	Stainless steel 316L + PTFE-graft	18 8	0.14 0.3	0.0258 0.0230	0.0001825 0.0002874
NIR Royal	Boston Scientific, Ratingen, Germany	Stainless steel 316LS + Gold-coating	26	0.102–0.109	0.0394	0.000193

PTFE = polytetrafluorethylene, DLC = diamond like carbon.

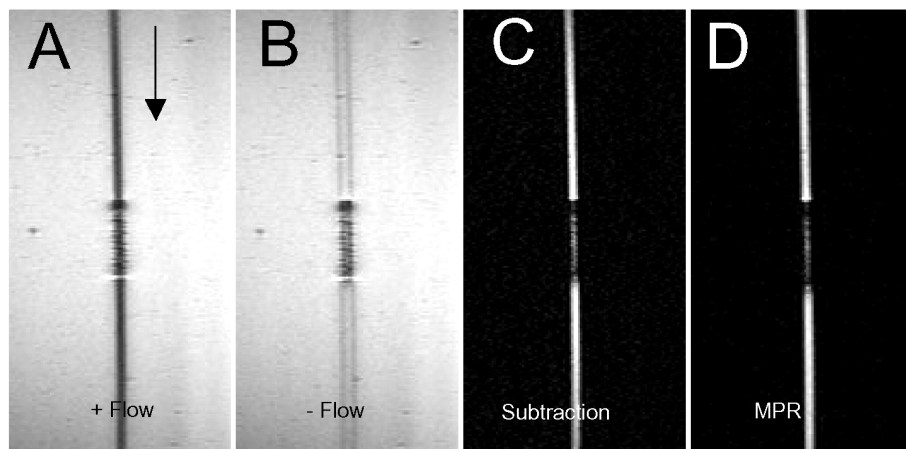


**Figure 1.** Demonstration of the method at the example of the Crossflex stent: Images with (A) and without (B) flow were acquired and subtracted. Subtraction images (C) show only flow signal, which is decreased in the stented area by artifacts. Signal intensity analyses were performed on MPR images (D).

### Image Postprocessing and Analysis

From the subtraction images, 4 mm thick multiplanar reformats (MPR) were obtained on the system console. Signal measurements were performed on the MPR images. Rectangular regions of interest (ROIs) of  $39 \text{ mm}^2$  were localized inside the stent, in the unstented part of the vessel, and in the background.

For objective quantitative data on the intraluminal signal properties, the contrast-to-noise ratio (CNR) between the stent lumen and the unstented region of the vessel were assessed. The CNR was defined as mean signal intensity (SI) inside the stent minus the mean SI in the vessel outside the stent divided by the standard deviation of the background signal. The signal-to-noise ratio (SNR) was defined as mean SI in the vessel outside the stent divided by the standard deviation of the background signal. To obtain an estimate of the signal attenuation of the individual stents, the CNR between the unstented part of the vessel and the background was also quantified.

Quantitative correlation of the given parameters strut thickness and volume/mm with the dependent parameters CNR and SNR was obtained by a linear regression analysis.

## RESULTS

Figure 1 demonstrates the results of one example stent (Crossflex) and the method applied for all stents.

Subtraction of images with and without flow results in an image in which only regions of flow are displayed with high SI.

Table 2 summarizes the quantitative data obtained in the 19 stents. The Wiktor stent (tantalum) showed the highest

**Table 2**  
*Results of the Signal Evaluations*

Name	CNR Stent	CNR BG	SNR Vessel
Wiktor	7.05	57.89	57.66
Radius	26.13	48.23	48.19
ACS RX Multilink	31.36	47.84	47.6
Crossflex	40.64	56.35	56.34
Sirius Carbostent	45.44	55.35	55.11
ML Tetra	46.06	56.96	56.66
Herculink	46.32	53.64	53.46
ML Tristar	47.35	56.45	56.34
V-Flex Plus	49.69	59.16	58.94
be-Stent	54.86	60.22	60.04
BiodivYsio	54.86	60.28	60.07
Flex AS	55.87	62.45	62.25
Jostent Flex	55.87	68.08	67.78
Palmaz-Crown	56.36	59.77	59.5
NIR Primo	56.5	58.32	58.11
Palmaz	56.7	61.45	61.16
Bx-Velocity	57.9	59.88	59.63
Jostent StentGraft	58.85	60.96	60.73
NIR Royal	60.05	61.52	61.27

intraluminal signal of all evaluated stents. With a CNR of 7, the intraluminal signal attenuation was minor when compared to the unstented vessel part and relatively homogeneous. Figure 2 compares the MPR images of all stents (except for the Crossflex, shown in Fig. 1). Consistent with the low CNR, the region of the Wiktor stent can barely be distinguished from the unstented “vessel” part. The Radius stent (nitinol) showed reduced intraluminal signal when compared to the Wiktor stent, but an increased CNR when compared to the steel stents. The signal also appears less homogeneous with a stripe structure.

Stents made of 316L stainless steel were associated with the largest local artifacts, but the degree of intraluminal signal reduction varied among the stent types. The ACS Multilink and the Crossflex showed the lowest signal attenuation among the steel stents. In these cases, the lumen appeared narrowed and the intraluminal signal was reduced when compared to the nonstented portion of the vessel while the majority of the lumen still remains visible. In the Sirius, Tetra, Herculink, Tristar, V-Flex, be-Stent,

Biodivisio, Flex AS, Jostent, Palmaz-Crown, NirPrimo, and Palmaz stents, the intraluminal signal attenuation was more pronounced, the signal was more inhomogeneous, feigned lumen narrowing was more evident, (e.g., be-Stent) and the lumen was not visible in its whole length (in the Herculink only in the middle). In the Nir Royal, the Velocity, and the Jograft, artifacts were most pronounced resulting in obscurity or even signal loss of the major parts of the stent lumen.

Not only the underlying material but also the stent design seemed to have influenced the extent of artifacts as indicated by the different results among different stainless steel stents. Nevertheless, the linear regression analysis of the specific stent design features strut thickness and the volume of the stent material per mm stent length with the measured variables CNR and SNR did not reveal a correlation ( $r$ -values  $< 0.5$ , see Fig. 3). The relative attenuation of the stented vessel segment when compared to the background CNR allowed an estimate of the “performance” of the stents. In the stainless steel stents with the largest artifacts, the CNR

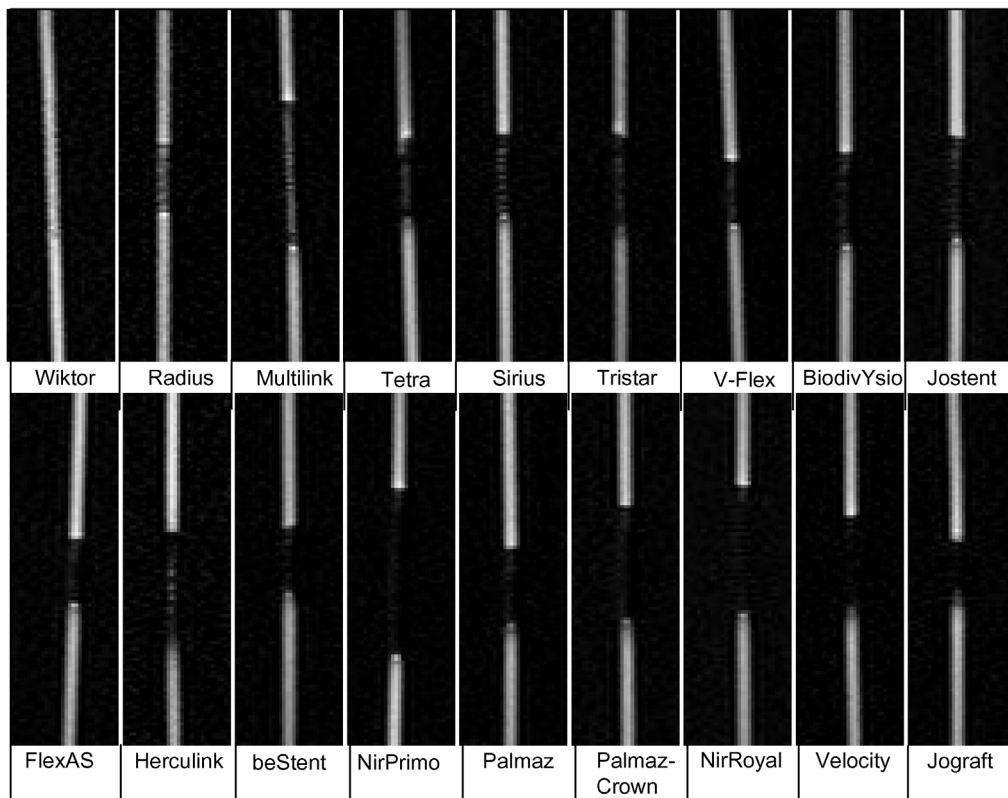


**Figure 2.** The MPR images of all examined stents. Note minor artifacts of the Wiktor stent (tantalum), relatively high signal intensity inside the Radius stent (nitinol) and varying degree of signal loss inside of the steel stents.

almost approached the CNR of the background, indicating near complete signal loss. However, signal attenuation as a function of these parameters was not consistent among the investigated stents.

**DISCUSSION**

This study includes a phantom evaluation of intraluminal signal properties of coronary artery stents.

Metallic stents are known to cause artifacts in MR. These artifacts are promoted by local magnetic field inhomogeneities and eddy currents. In addition, signal attenuation within the stent is caused by radio frequency (RF) shielding of the metallic stent material. Induced eddy currents in the stent may also lead to a lower nominal RF excitation angle inside the stent. This has shown to attenuate the signal acquired by the receiver coil.<sup>[10,11]</sup> Artifact-related signal changes may include signal voids or local signal enhancements

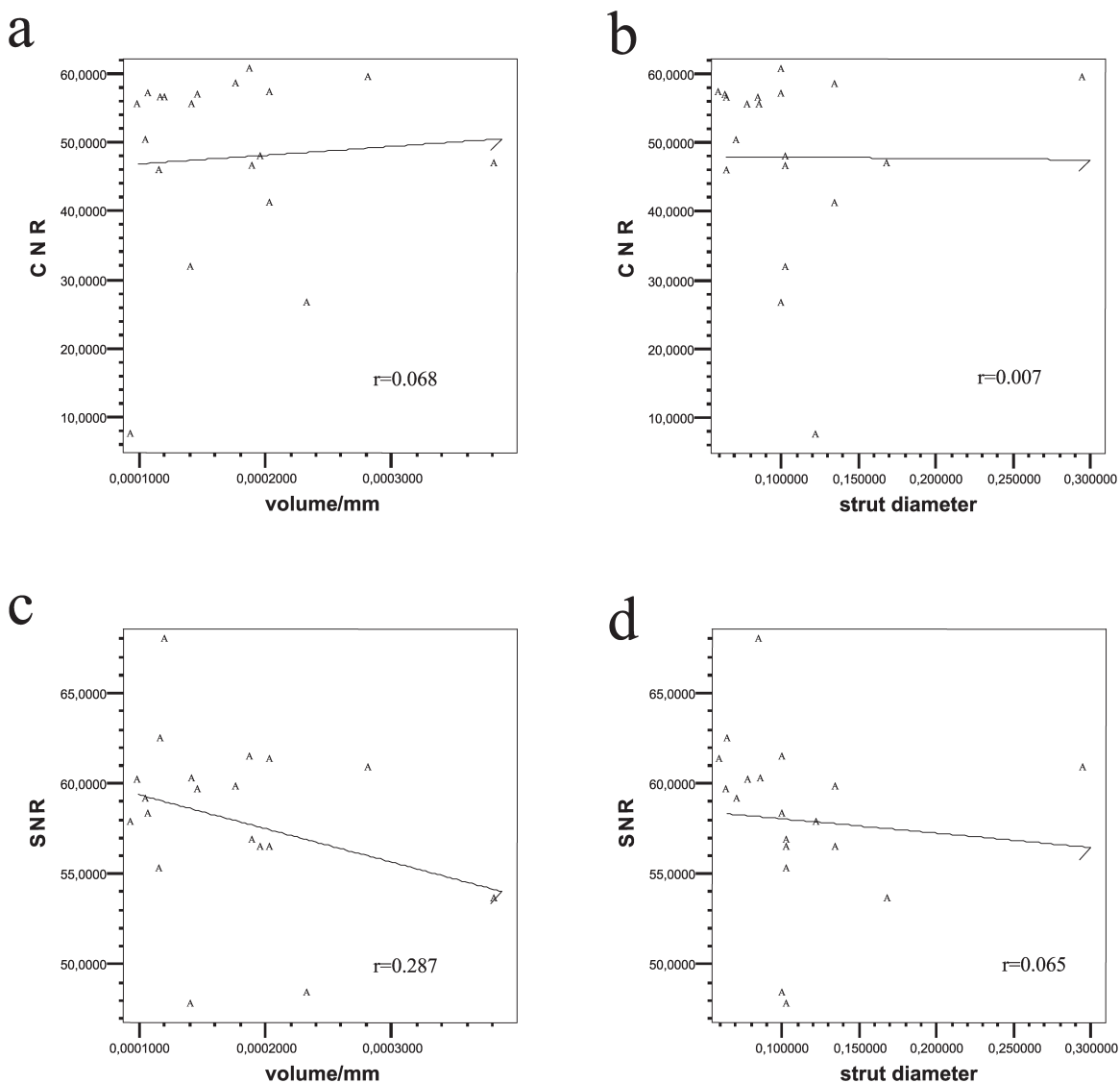


**Figure 3.** Linear regression analysis of the signal measurements (CNR, SNR) vs. strut thickness and the volume of the stent-material/mm.  $r$ -values  $< 0.5$  indicate no correlation of variables.

(mostly on fast spin-echo images). In our evaluation of intraluminal signal properties, we used a subtraction technique to suppress local artifactual signal enhancement. Subtraction of images acquired with and without flow only display flow-related signal changes while susceptibility artifacts with high signal are subtracted. Intraluminal signal loss caused by artifacts would result in narrowing of the stent lumen and reduced CNR inside the stent lumen; extraluminal artifacts could not be evaluated with this method. Although the subtraction technique would not be practical in an in vivo setting, it was well suited for the evaluation of RF signal penetration in the presence of various coronary stents. A further development for in vivo measurements may still be required.

Current coronary MRA techniques comprise a large array of different imaging sequences including fast spin-echo, gradient echo sequences, echo planar imaging, spiral imaging (see Ref. [12] and references therein). Our evaluations were carried out with a black-blood fast spin-echo imaging technique. This technique is associated with smaller “metallic” artifacts than conventional gradient-echo bright blood coronary MR angiography<sup>[13]</sup> and was chosen to imitate a best case scenario. The use of a constant flow phantom instead of a pulsatile flow phantom constitutes a limitation of this study. However, the contribution of flow to the total magnitude of artifacts is minor when compared to the contribution of susceptibility.<sup>[10]</sup>

Our examinations demonstrate retained high intraluminal signal inside the Wiktor stent (tantalum), moderate signal attenuation with good lumen visibility in the Radius stent (nitinol), and signal decrease of varying expression in the steel stents. In evaluations of iliac artery stents, a similar dependency of artifact expression on the underlying stent material has been demonstrated.<sup>[11,14]</sup> Hug et al. have compared different coronary artery stents regarding the total volume size of their artifacts in different imaging sequences.<sup>[8]</sup> Consistent with our findings, they found the smallest artifacts in the Wiktor tantalum stent using a black-blood fast spin-echo imaging sequence. A nitinol stent was not included in their series and imaging, nor did they report imaging of the stent lumen itself.

Our experiments were carried out with the stents oriented parallel to the main magnetic field ( $B_0$ ). Different stent orientations would have an influence on the expression of artifacts. In iliac artery stent evaluations orthogonal or diagonal orientations of the

stent in relation to  $B_0$  showed an increase in artifact size.<sup>[15]</sup> Duerinckx et al. have shown that the patency of Palmaz stents can be assessed indirectly by MRA in vivo by receiving flow signal in the coronary artery distal to the stent.<sup>[16]</sup>

While the Wiktor stent had the most favorable image characteristics, it can be found only in a small number of patients and is no longer commercially available. The vast majority of currently implanted stents are made of stainless steel. Since the lumina of these stents cannot be imaged reliably and a large increase in coronary MRA examinations may be expected, there is a need of research for alternative stent designs. Potential new stent-materials include novel metal alloys such as ABI alloy that showed less artifacts than steel, nitinol, or tantalum.<sup>[17]</sup>

Alternative developments may include bio-compatible and potentially artifact-free materials such as chitosan (a derivative of chitin, a polysaccharide found in the exoskeleton of shellfish as shrimp, crab, lobster),<sup>[18]</sup> polyurethane as already used for nasolacrimal stents,<sup>[19]</sup> polyethylene terephthalate as used for tracheal stents and under investigation for vascular applications,<sup>[20]</sup> cartilage stents created from chondrocytes for urethral stents,<sup>[6]</sup> or bioresorbable polyesters like poly(D,L-lactide).<sup>[21]</sup>

Besides more suitable materials for MRI, the arrangement, size, and geometry of the stent filaments remain to be studied. Among stents made from the same underlying material, differences in artifact expression may be attributed to the stent design and their resultant electrodynamic properties. While it might be expected that artifacts are reduced by thinner stent struts, larger distance between the struts and lower total volume of stent material, no consistent dependency on these parameters was observed in our series of stainless steel stents.

Finally, another interesting approach to image the stent lumen would be to use the stent as a receiver coil itself. Promising preliminary results with this technique were reported by Quick et al.,<sup>[22]</sup> but remains to be more fully explored.

In summary, coronary artery stents are sources of artifacts in MRA that superimpose the stent lumen to various degrees. The lumen of nitinol and especially Tantalum stents may be visualized. Future stent design should be focused on both the mechanical as well as the MR imaging characteristics. The MR method used in this article may also be helpful for the evaluation of future stent developments regarding their MR imaging suitability.

### ACKNOWLEDGMENTS

The authors would like to thank the following companies for their support: Boston Scientific, Ratingen, Germany; Cook, Mönchengladbach, Germany; Cordis, Haan, Germany; Guidant, Giessen, Germany; Jomed, Rangendingen, Germany; Krauth Medical, Hamburg, Germany (BiodivYsio stent); Medtronic, Düsseldorf, Germany; Phytis, Berlin, Germany; Stoeckert, Munich, Germany (Sirius Carbostent).

Furthermore, the authors thank the foundation Innovative Medizinische Forschung for supporting D.C. Maintz in his work.

David Maintz is supported in part by a grant from the Förderprogramm Innovative Medizinische Forschung (MA 610102), Münster, Germany.

### REFERENCES

1. Topol, E.J. Coronary-Artery Stents—Gauging, Gorging, and Gouging. *N. Engl. J. Med.* **1998**, *33*, 1702–1704.
2. Kastrati, A.; Schomig, A.; Elezi, S.; Schuhlen, H.; Dirschinger, J.; Hadamitzky, M.; Wehinger, A.; Hausleiter, J.; Walter, H.; Neumann, F.J. Predictive Factors of Restenosis After Coronary Stent Placement. *J. Am. Coll. Cardiol.* **1997**, *30*, 1428–1436.
3. Kastrati, A.; Mehilli, J.; Dirschinger, J.; Pache, J.; Ulm, K.; Schuhlen, H.; Seyfarth, M.; Schmitt, C.; Blasini, R.; Neumann, F.J.; Schomig, A. Restenosis After Coronary Placement of Various Stent Types. *Am. J. Cardiol.* **2001**, *87*, 34–39.
4. Serruys, P.W.; Emanuelsson, H.; van der Giessen, W.; Lunn, A.C.; Kiemeny, F.; Macaya, C.; Rutsch, W.; Heyndrickx, G.; Suryapranata, H.; Legrand, V.; Goy, J.J.; Materne, P.; Bonnier, H.; Morice, M.C.; Fajadet, J.; Belardi, J.; Colombo, A.; Garcia, E.; Ruygrok, P.; de Jaegere, P.; Morel, M.A. Heparin-Coated Palmaz-Schatz Stents in Human Coronary Arteries. Early Outcome of the Benestent-II Pilot Study. *Circulation* **1996**, *93*, 412–422.
5. Fenton, S.H.; Fischman, D.L.; Savage, M.P.; Schatz, R.A.; Leon, M.B.; Baim, D.S.; King, S.B.; Heuser, R.R.; Curry, R.C., Jr.; Rake, R.C. Long-Term Angiographic and Clinical Outcome After Implantation of Balloon-Expandable Stents in Aortocoronary Saphenous Vein Grafts. *Am. J. Cardiol.* **1994**, *74*, 1187–1191.
6. Amiel, G.E.; Yoo, J.J.; Kim, B.S.; Atala, A. Tissue Engineered Stents Created from Chondrocytes. *J. Urol.* **2001**, *165*, 2091–2095.
7. Shellock, F.G.; Shellock, V.J. Metallic Stents: Evaluation of MR Imaging Safety. *Am. J. Roentgenol.* **1999**, *173*, 543–547.
8. Hug, J.; Nagel, E.; Bornstedt, A.; Schnackenburg, B.; Oswald, H.; Fleck, E. Coronary Arterial Stents: Safety and Artifacts During MR Imaging. *Radiology* **2000**, *216*, 781–787.
9. Stuber, M.; Botnar, R.M.; Spuentrup, E.; Kissinger, K.V.; Manning, W.J. Three-Dimensional High-Resolution Fast Spin–Echo Coronary Magnetic Resonance Angiography. *Magn. Reson. Med.* **2001**, *45*, 206–211.
10. Bartels, L.W.; Smits, H.F.; Bakker, C.J.; Viergever, M.A. MR Imaging of Vascular Stents: Effects of Susceptibility, Flow, and Radiofrequency Eddy Currents. *J. Vasc. Interv. Radiol.* **2001**, *12*, 365–371.
11. Maintz, D.; Kugel, H.; Schellhammer, F.; Landwehr, P. In Vitro Evaluation of Intravascular Stent Artifacts in Three-Dimensional MR Angiography. *Investig. Radiol.* **2001**, *36*, 218–224.
12. Botnar, R.M.; Stuber, M.; Dianas, P.G.; Kissinger, K.V.; Bornert, P.; Manning, W.J. Coronary Magnetic Resonance Angiography. *Rev. Cardiol.* **2001**, *9*, 77–87.
13. Stuber, M.; Botnar, R.M.; Kissinger, K.V.; Manning, W.J. Free-Breathing Black-Blood Coronary MR Angiography: Initial Results. *Radiology* **2001**, *219*, 278–283.
14. Lenhart, M.; Volk, M.; Manke, C.; Nitz, W.R.; Strotzer, M.; Feuerbach, S.; Link, J. Stent Appearance at Contrast-Enhanced MR Angiography: In Vitro Examination with 14 Stents. *Radiology* **2000**, *217*, 173–178.
15. Klemm, T.; Duda, S.; Machann, J.; Seekamp-Rahn, K.; Schnieder, L.; Claussen, C.D.; Schick, F. MR Imaging in the Presence of Vascular Stents: A Systematic Assessment of Artifacts for Various Stent Orientations, Sequence Types, and Field Strengths. *J. Magn. Reson. Imaging* **2000**, *12*, 606–615.
16. Duerinckx, A.J.; Atkinson, D.; Hurwitz, R. Assessment of Coronary Artery Patency After Stent Placement Using Magnetic Resonance Angiography. *J. Magn. Reson. Imaging* **1998**, *8*, 896–902.
17. van Dijk, L.C.; van Holten, J.; van Dijk, B.P.; Matheijssen, N.A.; Pattinama, P.M. A Precious Metal Alloy for Construction of MR Imaging-Compatible Balloon-Expandable Vascular Stents. *Radiology* **2001**, *219*, 284–287.
18. Lauto, A.; Ohebshalom, M.; Esposito, M.; Mingin, J.; Li, P.S.; Felsen, D.; Goldstein, M.; Poppas, D.P. Self-Expandable Chitosan Stent: Design and Preparation. *Biomaterials* **2001**, *22*, 1869–1874.
19. Lanciego, C.; De Miguel, S.; Perea, M.; Cano, C.; Garcia, I.R.; Davila, J.; Ibarburen, C.; Toledano, N.; Rodriguez-Merlo, R.; Garcia, L.G. Nasolacrimal Stents in the Management of Epiphora: Medium-Term Results of a Multicenter Prospective Study. *J. Vasc. Interv. Radiol.* **2001**, *12*, 701–710.
20. De Scheerder, I.K.; Wilczek, K.V.; Verbeken, E.V.; Barios, L.; Piessens, J.; De Geest, H. Intraarterial Biocompatibility of Polyethylene Terephthalate Self-

- Expandable Stents Implanted in Porcine Peripheral Arteries. *Acad. Radiol.* **1995**, 2, 154–158.
21. Blindt, R.; Hoffmeister, K.M.; Bienert, H.; Pfannschmidt, O.; Bartsch, G.; Thissen, H.; Klee, D.; Vom Dahl, J. Development of a New Biodegradable Intravascular Polymer Stent with Simultaneous Incorporation of Bioactive Substances. *Int. J. Artif. Organs* **1999**, 22, 843–853.
  22. Quick, H.; Ladd, M.; Nanz, D.; Mikolajczyk, K.; Debatin, J. Vascular Stents as RF Antennas for Intravascular MR Guidance and Imaging. *Magn. Reson. Med.* **1999**, 42, 738–745.

Received February 8, 2002

Accepted April 24, 2002